◆ Human Brain Mapping 11:12–32(2000) ◆

# Three-Dimensional Mapping of Cortical Thickness Using Laplace's Equation

**Stephen E. Jones,[1]* Bradley R. Buchbinder,[2] and Itzhak Aharon[3]**

[1]*Tufts University School of Medicine*
[2]*Division of Neuroradiology, Department of Radiology, Massachusetts General Hospital*
[3]*Department of Neuroradiology, Massachusetts General Hospital*

**Abstract:** We present a novel, computerized method of examining cerebral cortical thickness. The normal cortex varies in thickness from 2 to 4 mm, reflecting the morphology of neuronal sublayers. Cortical pathologies often manifest abnormal variations in thickness, with examples of Alzheimer's disease and cortical dysplasia as thin and thick cortex, respectively. Radiologically, images are 2-D slices through a highly convoluted 3-D object. Depending on the relative orientation of the slices with respect to the object, it is impossible to deduce abnormal cortical thickness without additional information from neighboring slices. We approach the problem by applying Laplace's Equation ($\nabla^2\psi = 0$) from mathematical physics. The volume of the cortex is represented as the domain for the solution of the differential equation, with separate boundary conditions at the gray-white junction and the gray-CSF junction. Normalized gradients of $\psi$ form a vector field, representing tangent vectors along field lines connecting both boundaries. We define the cortical thickness at any point in the cortex to be the pathlength along such lines. Key advantages of this method are that it is fully three-dimensional, and the thickness is uniquely defined for any point in the cortex. We present graphical results that map cortical thickness everywhere in a normal brain. Results show global variations in cortical thickness consistent with known neuroanatomy. The application of this technique to visualization of cortical thickness in brains with known pathology has broad clinical implications. *Hum. Brain Mapping 11:12–32, 2000.* 

**Key words:** cortex; MRI; thickness; brain

## INTRODUCTION

The cerebral cortex is a topological shell of gray matter surrounding a core of white matter with a normal thickness of typically 3 mm [Henery et al., 1989; Paxinos, 1990, and the classic reference by von Economo, 1925]. Variations in thickness can be either physiological or pathological. Physiologic variations depend on the location of the cortex, roughly ranging from 2 mm in the calcarine cortex to 4 mm in the precentral gyrus. Pathological variations are associated with many diseases and can be either localized or global. Examples of increased pathological thickness are cortical dysplasias and lissencephaly [Lee et al., 1998], and examples of thinner pathological cortex are Alzheimer's disease [Double et al., 1996; Grignon et al., 1998; Tanabe et al., 1997], schizophrenia [Kwon et al., 1999], and anorexia nervosa [Lambe et al., 1997]. Presently, there are no satisfactory methods for determining cortical thickness in vivo, although other efforts are underway [Zeng et al., 1999]. The brain's highly convoluted folding in three dimensions precludes accurate analysis from radiological studies, which typically dis-

*Correspondence to: Stephen Jones, 97 Hoitt Rd, Belmont, MA 02478. E-mail: sjones@opal.tufts.edu

Received for publication 25 October 1999; accepted 22 May 2000

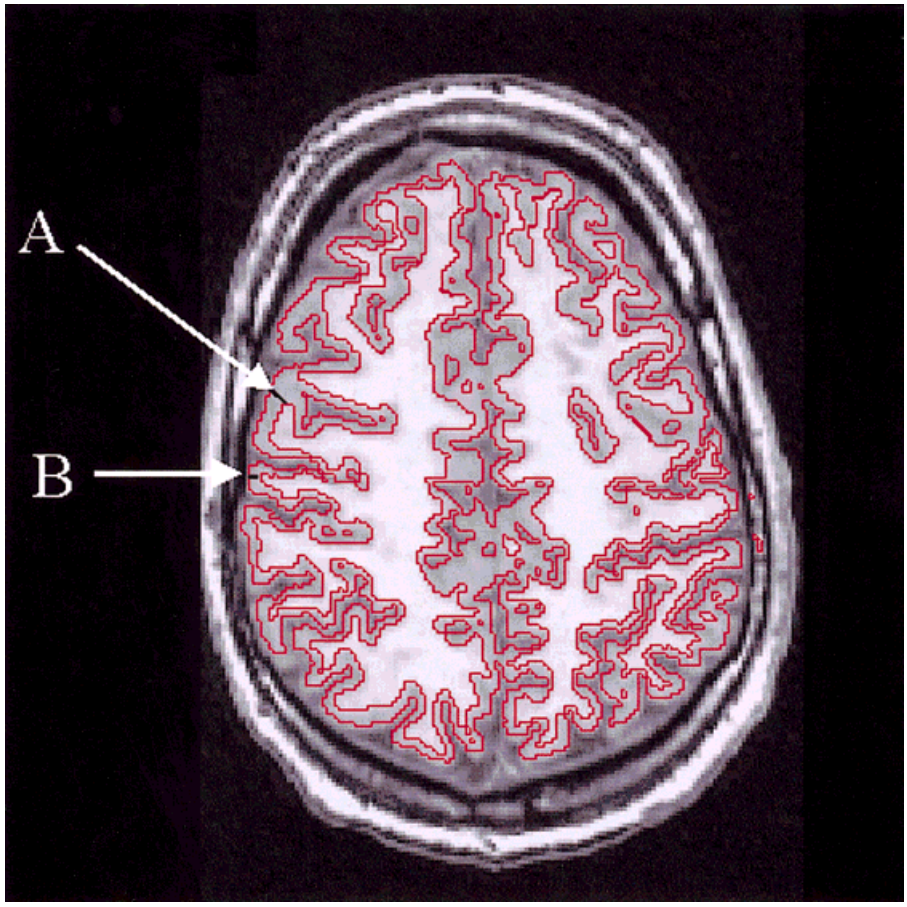


**Figure 1.**
Example of a raw axial T1 MRI image with superimposed segmentation of cortex. Although the cortex indicated at point **A** appears thicker than that indicated at point **B**, subsequent analysis reveals their thickness to be almost identical. The discrepancy is an artifact of the three dimensional angle of intersection between the axial slice and the cortical surface.

play two-dimensional slices at variable orientations with respect to the cortical shell.

There is scientific and clinical value for any method computing the global three-dimensional thickness of the cortex from radiological studies. A clinical example could be a tentative diagnosis of focal epilepsy given evidence of a pathological increase in cortical thickness due to a cortical dysplasia. Another example could be the early diagnosis of Alzheimer's disease if the pattern of cortical thinning could be documented. These examples serve as the motivation for this paper, that is, to develop a tool used by radiologists and researchers to accurately map the three-dimensional cortical thickness over the entire cortical volume, using state-of-the-art radiological images.

Currently, methods to determine cortical thickness rely on a radiologist's skill in extrapolating the three-dimensional thickness from a series of two-dimensional images. This requires estimating the angle between the intersecting imaging plane and the cortical tangent plane. The difficulty can be appreciated with an example shown in Figure 1, which is an axial T1 weighted MR image showing segmented gray matter. The inner and outer boundaries of the gray matter are overlaid with white lines, thereby "segmenting" the cortex. A brief estimation of the cortical thickness of the regions labeled A and B leads to the erroneous conclusion that A is thicker than B, when in fact they are nearly the same thickness. Unless it is known that the image plane lies orthogonal to both cortical surfaces, it is impossible to determine the thickness without information from neighboring slices. Similar difficulties are encountered in experimental studies of the rat's cortical thickness [Braitenberg, 1998]. Occasionally, standard image planes are known to be roughly orthogonal to areas of cortex and thickness estimates can be visually derived, for example using axial images of the central sulcus [Meyer et al., 1996] or interhemispheric fissure. However, none of these tricks can work in all areas of the brain at the same time without a more involved analysis. Such an analysis is inherently data intensive, given the ratio of cortical thickness to cerebral diameter and the three-dimensional nature of the problem. It is the purpose of this paper to present such a method, now made possible by the

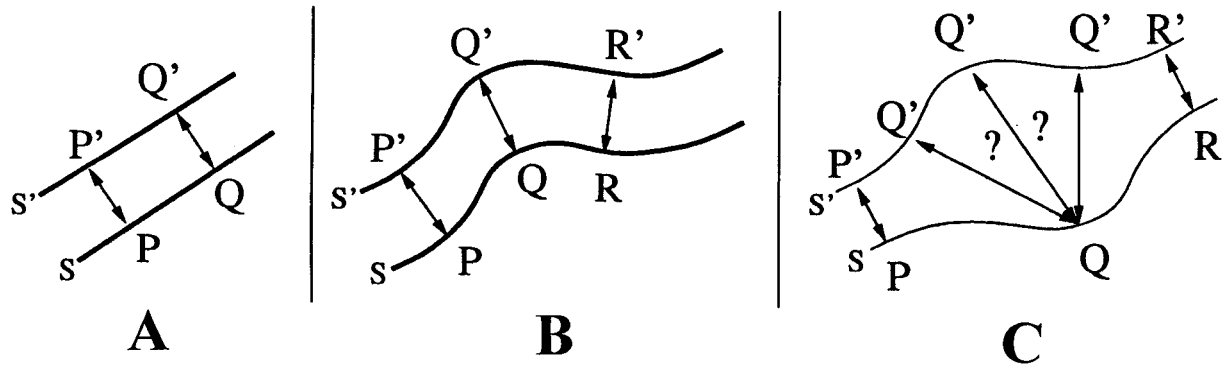


**Figure 2.**

Three two-dimensional examples of thickness in different geometries. Panel **A** shows the thickness between two boundaries of parallel straight lines as orthogonal projections (e.g., lines P–P′ and Q–Q′ are perpendicular to both S and S′). Panel **B** also uses orthogonal projections but the boundaries are curvilinear with the distance between them much smaller than their radius of curvature. Panel **C** has two boundaries where the distance between them in not much smaller than their radius of curvature. The thickness based on orthogonal projections is compatible with example pathlengths P–P′, and R–R′, but not at pathlengths originating from point Q.

recent availability of high resolution MRI and powerful computers.

The rest of this paper is outlined as follows. The Methods section discusses the problem of defining cortical thickness and describes an approach using solutions from Laplace's equation. The Results section applies the Laplace method to MRI data from a normal brain culminating in a three-dimensional mapping of the cortical thickness. The results are compared to results from known neuroanatomy. The method is also extended into "supracortical" volumes outside of the gray-CSF surface to provide a robust definition for the "depth" of infolded cortex from an outside surface such as the dura. Display algorithms are described which allow one to look into sulcal folds and observe trends in thickness variations. The paper concludes with a discussion of the method, indicating its general nature and powerful applicability.

## METHODS

Given the goal of mapping the three-dimensional cortical thickness everywhere in the brain, there are two major problems to address: (1) a definition of thickness which is robust in the highly variable and convoluted cortical environment, and (2) a similarly robust and rigorous mathematical algorithm to compute thickness using that definition from available imaging studies.

### Definition of thickness

We start by abstracting the cortex of each hemisphere to be a volume bounded by two surfaces, S and S′. We assume S and S′ are topologically equivalent to a sphere, that is although they are highly convoluted they can be abstractly stretched and warped without breaking to form the surface of a sphere. (Strictly, the cortex from each hemisphere is topologically a sheet, but for computational and display purposes, the hole caused by the brainstem region is "capped," thereby creating a topologically spherical cortex.) The term "thickness" has two implicit and separate notions. (1) Thickness is always measured between a point on S and another point on S′. That is, there is an *association* of any point P on S with some point P′ on S′. (2) Given the pair of points P and P′, there is some definition of "distance" or "thickness" between them. In Euclidean 3-space, the distance is the length of the straightline segment between them. Figure 2, illustrates these notions with three two-dimensional examples. Figure 2a assumes S and S′ are straight and parallel. A natural, or intuitive, mapping from one surface to the other uses the perpendicular projection, and a natural thickness is the straightline distance between the pairs of points. These definitions also provide four intuitive and desirable properties for a rigorous and robust mathematical method: (1) every point on S has a defined mapping and thickness, (2) the mappings are one to one, that is every point in S is mapped to only one point in S′, and no point in S′ has more than one point mapped onto it, (3) reciprocity such that the pairs of points and the resulting thickness are the same whether you start from P and map to P′ or if you start with P′ and map to P, and (4) the distance is the minimum of all possible pairs of P and P′. Figure 2b shows a similar example where S and S′ are still

quasi-parallel but no longer straight. This example also provides the same four valuable properties as the previous example. However, Figure 2c shows an example of a varying thickness where the above definitions encounter difficulty and no longer satisfy the three properties. The mapping from P to P′ and R to R′ might make sense, but not for points like Q, which represents the majority of points on S in this example. It is not intuitively clear which point Q′ is the best mapping for Q. Also, a projection from Q orthogonal to S is no longer guaranteed to be orthogonal to S′ at Q′ (thus reciprocity is lost). This difficulty becomes amplified as we analyze real examples in three dimensions.

There are two definitions of thickness with natural motivations. The first approach derives from anatomic measurements on cadaveric brains, where a depth gauge is inserted through cortex being perpendicular to the gray-CSF surface. The thickness is read as the depth when the gauge reaches the gray-white surface. The second approach derives from a minimization principle where the thickness at any point on the gray-CSF surface is defined as minimum distance of a straight line to any point on the gray-white surface. This condition is met when the straight line intersects the gray-white surface perpendicularly. A two-dimensional schematic of these definitions is shown in Figure 3 for the example of Figure 2c. The first mapping (Fig. 3a) uses the orthogonal projection from S to S′ (that is, the straight line from P to P′ is perpendicular to the surface at S). This mapping has three problems: the straight-line distance from P to P′ can seem intuitively too long, there is a loss of reciprocity from P′ to P as P′ maps to P″, and another point Q could map to the same point P′. The approach in Figure 3b finds the closest point on S′ to P. This is equivalent to finding a point P′ such that the straight line from P to P′ is perpendicular to the surface at S′. But this definition encounters the same problems as the first: the straight-line distance from P to P′ can seem intuitively too long, there is a loss of reciprocity, and a loss of uniqueness.

To conclude, the intuitive and simple definitions that applied well to Figure 2a and b and provided three rigorous mathematical properties, cannot be applied to examples like Figure 2c and yield simultaneously the same mathematical properties. Applied to the cortex, the simple definitions are probably good enough if the cortex is thin and gently curves, but fail in regions of high convolutions or rapidly varying thickness. Put mathematically, if R and R′ are the radii of curvature for P and P′ with $\Delta R = R - R'$, simple definitions apply when $\Delta R/R \ll 1$. (Rigorously, for any value of $\Delta R/R$, the simple definitions apply in the special case where the radius of curvature *vectors* of P and P′ are colinear).

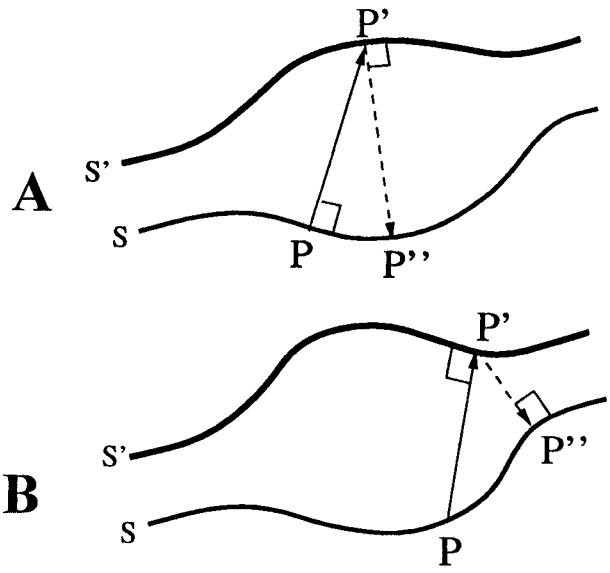


**Figure 3.**
Two candidate definitions for thickness in a two-dimensional example based on one orthogonal intersection. Panel **A** assumes an orthogonal projection from S which crosses to intersect S′, as exemplified by P–P′. Not the lack of reciprocity as the orthogonal projection from P′ does not return to P′. Panel **B** assumes a projection from S that crosses to orthogonally intersect S′. This is equivalent to finding the point P′ on S′ closest to a given point P lying on S. Again, there is a lack of reciprocity.

Therefore, we seek a new definition of mapping and thickness which preserves the mathematical properties provided by examples Figure 2a and b, yet is applicable in examples like Figure 2c. We approach regions like Figure 2c as composed of many nested sublayers and consider the thickness of each sublayer separately. In this limit $\Delta R/R$ is small for all sublayers and the simple definitions can be applied to each sublayer. The strategy is to define the overall thickness as the sum of the sublayer thickness. This approach preserves the desired rigorous mathematical properties when $\Delta R/R \ll 1$, and has an analogous association to known neuroanatomy where the cerebral neocortex is composed of six layers. Thus, we seek a method that describes a series of nested surfaces that can be smoothly deformed from S to S′. Such a series of surfaces is reminiscent of the equipotential surfaces used in the mathematical description of electrostatic fields. These surfaces are described by Laplace's equation. For the remainder of this paper we borrow this tool from mathematical physics and apply it to the problem of cortical thickness.

### Mathematical model for thickness

The centerpiece of this paper is the application of Laplace's equation to compute cortical thickness in concordance with the discussions above. Laplace's equation is fundamental to mathematical physics and has applicability over a broad range of phenomena. Examples include gravitational fields for celestial dynamics, electrostatic fields for particle acceleration, thermodynamic flows, any diffusion calculation, invicid incompressible fluid flow, and hydrostatics [Bland, 1965; Morse et al., 1953].

Laplace's equation is a second-order partial differential equation for a scalar field $\psi$ that is enclosed between boundaries S and S′. Mathematically, it takes the form

$$\nabla^2\psi = \frac{\partial^2\psi}{\partial x^2} + \frac{\partial^2\psi}{\partial y^2} + \frac{\partial^2\psi}{\partial z^2} = 0$$

where $\psi = \psi_1$ on S and $\psi = \psi_2$ on S′. Functions that satisfy Laplace's equation are called harmonic or potential functions. Harmonic functions have many beautiful mathematical properties. Included among them is an underlying geometric structure, which applies naturally to the definition of cortical thickness. For our example, Laplace's equation describes a layered set of nested surfaces that make a smooth transition from S to S′. This is the desired property for computing cortical thickness as described in the previous section.

Figure 4 shows a two-dimensional example of how Laplace's equation determines thickness. A "potential" $\psi$ is defined everywhere between the two lines such that $\psi = 0$ on S, $\psi = 10{,}000$ on S′, and $\nabla^2\psi = 0$ everywhere in between. The values of 0 and 10000 can be assigned units of volts, in analogy with electrostatic fields. Mathematically, the final pattern of streamlines is independent of the choice of boundary condition voltages, as long as the two voltages are different. The resulting profile of $\psi$ is a smooth transition from $\psi = 0$ V on S to $\psi = 10{,}000$ V on S′. The significant property of Laplace's equation is that nonintersecting intermediate lines, or isopotentials, with constant values between 0 V and 10,000 V must exist between S and S′. Examples are indicated as dashed lines for isopotential values of 2,500, 5,000, and 7,500 V. In effect, these intermediate lines divide the volume into any desired set of sublayers. Once the solution of $\psi$ is obtained, "field lines" are computed using

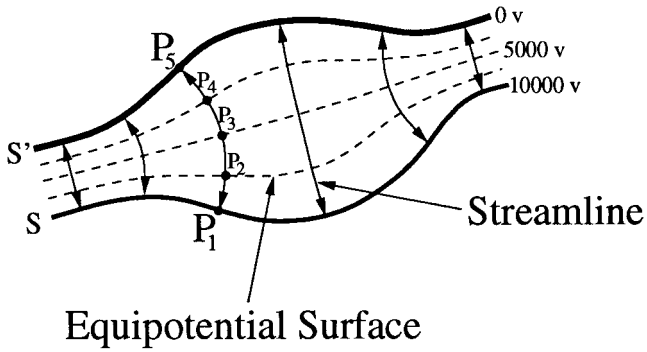


**Figure 4.**
Two-dimensional example of Laplace's method. Laplace's equation is solved between S and S′, which have predetermined boundary conditions of 10,000 V and 0 V, respectively. Three examples of resulting intermediate equipotential surfaces are indicated for 2,500 V, and 5,000 V, and 7,500 V. Field lines connecting S to S′ are defined as being everywhere orthogonal to all equipotential surfaces, as exemplified by the line connecting P to P′.

$$\mathbf{E} = -\nabla\psi$$

that is normalized to

$$\mathbf{N} = \mathbf{E}/\|\mathbf{E}\|$$

**N** represents a unit vector field defined everywhere between S and S′ which always points perpendicularly to the sublayer on which it sits.

After computing **N,** "field lines" or "streamlines" are computed by starting at any point on S and integrating **N.** For example, in Figure 4, consider starting at point $P_1$ and using a large integration step size. Integrating **N** takes you from $P_1$ to $P_2$ to $P_3$ to $P_4$ to $P_5$, with the five points forming a "streamline." The pathlength can be defined as the sum of straightline distances from $P_1$ to $P_2$ to $P_3$ to $P_4$ to $P_5$. Although this example crudely uses a total of four steps to cross from $P_1$ to $P_5$, any larger number of steps $n$ with smaller step size could be used to describe a curve from $P_1$ to $P_n$. The larger the number of steps, the more accurate the streamline fits an ideal curve. Mathematically, a curve which starts at $P_1$, ends at $P_n$, and has length $T$ is described by a vector function **C**(s) parameterized by s and defined by

$$\frac{d\mathbf{C}(s)}{ds} = \mathbf{N}(\mathbf{C}(s))$$

where **C**(0) is point $P_1$ and **C**(T) is point $P_n$.

As mentioned previously, the mathematical formalism of Laplace's equation underlies the description of

vastly different physical systems. Nevertheless, each system must share those properties of Laplace's equation that are mathematically guaranteed to occur. Among the properties are the following [Apostle, 1967; Morse et al., 1953]:

(1) Laplace's equation is manifestly three-dimensional and is, thus, independent of the coordinate system.

(2) The streamlines can never cross, although they can bifurcate in contrived conditions containing a saddlepoints where $\mathbf{E} = 0$ (i.e., a point of unstable equilibrium). The saddlepoint condition will not occur in our application to the cortex because the volume is bounded by two surfaces, each of which is continuous and enclosed. (Streamlines can cross if there is a "point source" in the interior, in which case Laplace's equation becomes Poisson's equation.)

(3) Any point P on S maps to a point P′ on S′, and P′ maps back to P, so reciprocity is automatic. From this follow two important corollaries: Every point on S is guaranteed to have a unique streamline ending at some point on S′, and every point on S′ is guaranteed to have a unique streamline ending at some point on S.

(4) Any and every point in the interior between S and S′ has a unique streamline going through it, connecting a pair of points on S and S′.

(5) Every streamline can be associated with its length and this can be used to define the thickness between P and P′.

(6) Properties 4 and 5 imply that every point between S and S′, inclusively, is associated with a thickness. Thus, the thickness can be defined in the volume rather than on a surface. This has implications for display purposes.

(7) The value of the thickness along a streamline is constant.

Aside from the mathematical properties, the concept of nested sublayers makes sense geometrically and anatomically. Further, computational methods solving Laplace's equation are simple and robust [Press et al., 1992].

## Computational method

All computer algorithms were written using IDL [Research Systems, Inc., 1998] and run on Sun Ultra II with 158 MB RAM and 1.5 GB swap space. IDL is a high level graphical language that allows fast and efficient development and debugging. IDL routines are optimized C programs that allow parallel-like computation with large data arrays.

Because multiple scans were often obtained at the same time, analysis begins by averaging all scans and compiling them into one three-dimensional dataset. Then the following nine steps are performed:

(1) Because raw MRI data includes all cranial structures, voxels corresponding to the cortical volume must be separated, or segmented, from all other voxels. The first step is to isolate the cerebrum, for which the skull, spinal cord, brainstem, orbits, and cerebellum are removed semi-automatically by using alternating cycles of the mathematical morphological operations erosion and dilation. In essence, with appropriate choice of thresholds, erosion cycles widen the gaps between cranial structures so they are no longer contiguous. Thus isolated, they can be removed. The remaining cerebral core is then de-eroded, or dilated, until restored to its pre-erosion state. Techniques to isolate the cerebrum from MRI images is an active field of research, to which we make no claim, and the interested reader is referred for details to the recent review and references in Dale et al. [1999].

(2) Although the data is acquired in a three-dimensional mode, there exist gradual slice-to-slice variations in signal intensity. Normalizing the gray matter peak (taken from the histogram of signal intensities) rescales the signal intensity for each slice to the mode of gray matter peaks from the entire brain. Interpolating normalization factors from interior slices solves difficulties encountered in extreme slices due to volume averaging.

(3) Within one slice, there exist low spatial frequency variations in signal intensity due to scanner inhomogeneities. The inhomogeneities are measured as the low order modes of a two-dimensional Fourier transform. The inverse transform of the low order modes forms a low-pass filtered image that can be used as a correction factor to rescale the initial image and thereby remove low-frequency nonuniformities. Although algorithmic details minimize volume averaging effects in the extreme slices, a three-dimensional Fourier transform is the ideal approach, which could not be implemented for this analysis.

(4) Because the voxel aspect ratio is typically nonuniform, the data are regridded using a trilinear interpolation to achieve a 1:1:1 aspect ratio. This is not computationally necessary, but makes coding and debugging easier.

(5) Because the cortex is folded so that opposing sides of a sulci may lie very close to each other, it is important to carefully segment the gray-CSF surface. If the gray-CSF boundary is missed in such regions, the cortex will seem to have at least twice the correct thickness. Often, raw MRI data does not have the

capability to fully resolve a small gap between opposing gray-CSF surfaces, so an algorithm is employed to estimate sulcal location by local examination around the sulcus. An average image is obtained using a boxcar, or local, average technique with a kernel that is much wider than the cortical thickness. The average image can be subtracted from the original image, using appropriate scaling factors, thereby amplifying regions with high frequency changes. Such regions include the small gaps between opposing gray-CSF surfaces. With optimal choice of scaling factors, the net result is to increase the contrast of sulcal regions by decreasing the signal intensity within the intervening CSF voxels. "Thinning" routines from image processing are then used to select these voxels and develop a skeleton image of the back-to-back gray-CSF surfaces within sulci. The skeleton is only one voxel wide, and can be subtracted from the original image to "scour" the sulci. This process does not improve the resolution, but it does improve the segmentation.

(6) Following all image corrections, the cortex is segmented using two thresholds for the gray-CSF surface and for the gray-white surface. Every voxel is then associated with one of three volumes, a cortical volume (gray matter), a white matter volume, and an extra-cerebral volume.

(7) The white matter volume is set to a fixed potential of 0, and the supra-cortical, or CSF, volume is set to a fixed potential of 10,000. Laplace's equation is solved iteratively throughout the entire data volume, keeping the white matter and CSF volumes fixed at 0 and 10,000, respectively. Computational methods to solve Laplace's equation are standard [Johnson et al., 1982; Press et al., 1992] and the simplest (the Jacobi method) takes the form

$$\psi_{i+1}(x,y,z) = [\psi_i(x + \Delta x,y,z) + \psi_i(x - \Delta x,y,z) + \psi_i(x,y + \Delta y,z) + \psi_i(x,y - \Delta y,z) + \psi_i(x,y,z + \Delta z) + \psi_i(x,y,z - \Delta z)]/6$$

where $\psi_i(x,y,z)$ is the value of the potential at $x,y,z$ during the $i$th iteration. Convergence is measured by the total field energy over all voxels

$$\varepsilon_i = \sum((\Delta\psi_i/\Delta x)^2 + (\Delta\psi_i/\Delta z)^2) + (\Delta\psi/\Delta z)^2)]^{1/2}$$

Iterations continue until the ratio $(\varepsilon_i - \varepsilon_{i+1})/\varepsilon_i$ becomes smaller than a preset threshold, typically about $10^{-5}$. Convergence usually occurs well under 200 iterations for data with 0.5 mm resolution.

(8) Gradients of $\psi$ are computed using simple two point differences, for example,

$$\Delta\psi(x,y,z)/\Delta x = [\psi(x + \Delta x,y,z) - \psi(x - \Delta x,y,z)]/2$$

All gradient vectors are normalized to produce the tangent vectors field **N,** for example,

$$N_x = (\Delta\psi/\Delta x)/[(\Delta\psi/\Delta x)^2 + (\Delta\psi/\Delta y)^2 + (\Delta\psi/\Delta z)^2)]^{1/2}$$

(9) The streamlines are computed for every voxel in the cortical volume. Every voxel acts as the origin for the streamline passing through it, going in one direction to the $V = 0$ surface and in the other direction on the $V = 10{,}000$ surface. The streamline is determined in two parts by integrating the tangent vector field using Euler's method, first from the voxel to the $V = 0$ surface, and then from the voxel to the $V = 10{,}000$ surface. Euler's method was chosen because of speed over a Runge-Kutta method. The two pathlengths are added together and define the thickness for the streamline passing through the voxel.

The illustrative examples so far have been in two dimensions. Figure 5 provides a three-dimensional example, which illustrates the concept of thickness as a volumetric measure. The top panel shows a small section of a brain to be highlighted. The middle panel amplifies that section of cortex as a mathematical shell, with an outer gray-CSF boundary set to 0 V and an inner gray-white boundary set to 10,000 V. Examples of intermediate sublayers at 7,500 V and 2,500 V are included. Although several examples are displayed of streamlines connecting the gray-CSF surface to the gray-white surface, the entire volume can be visualized as being filled with an infinite number of nonintersecting streamlines. Furthermore, each line can be associated with a number that is the length of that line, thereby providing a volumetric definition for cortical thickness.

### Laplace method in supracortical volume

The Laplace method has so far been applied to the cortical volume between the gray-CSF surface and the gray-white surface. The method is very general and can be applied to any volume that is bounded by two nonintersecting surfaces where the notion of mappings, trajectories, and intermediate surfaces apply. One such volume is the supracortical volume between the gray-CSF surface and an extracerebral surface, such as the inner calvarial surface. The exterior surface

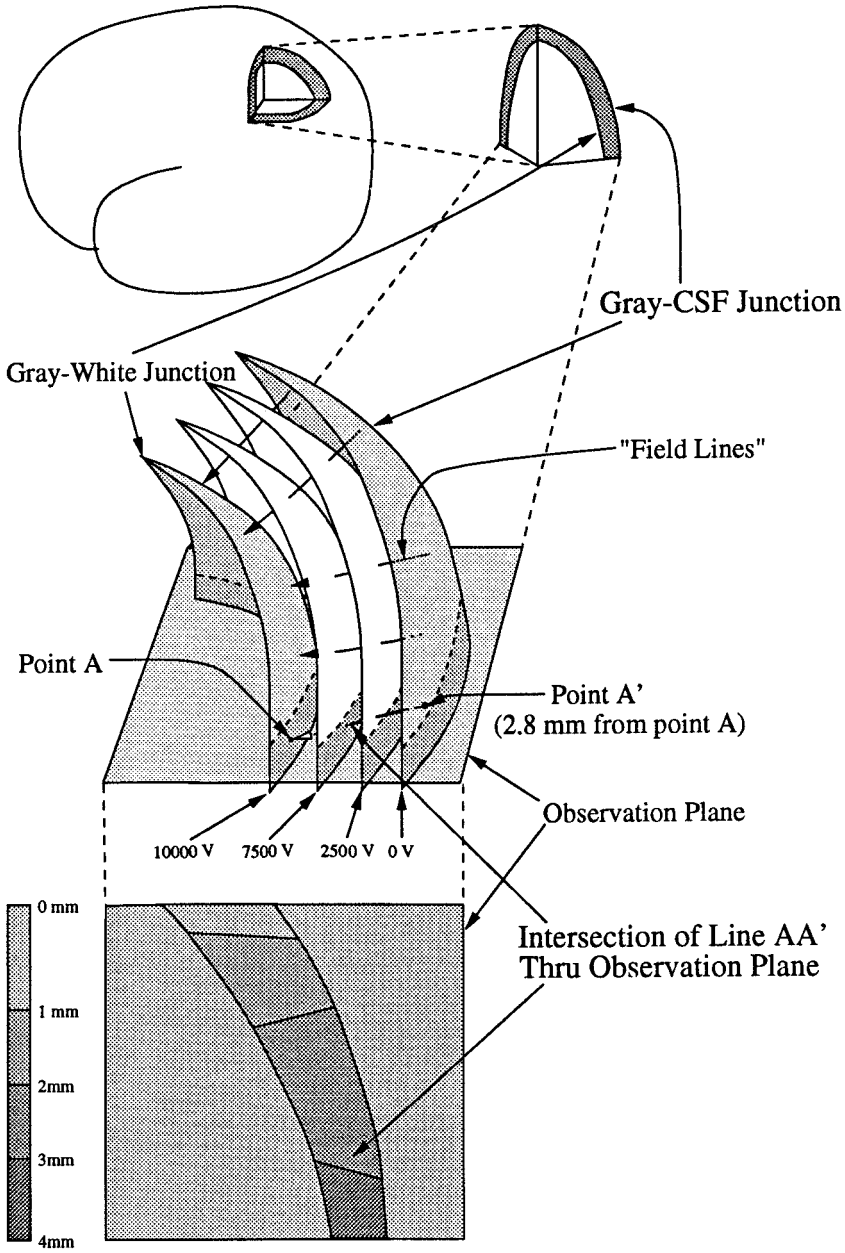


**Figure 5.**
Three-dimensional cartoon example of Laplace's method. The top panel shows a portion of cortex to be highlighted below. The middle panel converts that segment of cortex into a mathematical volume for Laplace's method. The gray-CSF surface and gray-white surfaces are fixed to boundary conditions of 0 V and 10,000 V, respectively, and Laplace's equation is solved in between. Two examples of resulting intermediate equipotential surfaces are indicated for 2,500 V and 7,500 V. Five example field lines are indicated connecting the two surfaces, which are everywhere orthogonal to all intermediate equipotential surfaces. The cortical thickness is defined anywhere in the cortical volume as the thickness of the field line passing through that point and connecting the two surfaces. The cortical volume intersects an "observation plane," on which thickness results are mapped for tomographic visualization as exemplified in the bottom panel. For example, the line A–A′, with a pathlength of 2.8 mm, happens to intersect the observation plane. That region of the observation plane is then color-coded for 2.8 mm with respect to the color bar.

is formed computationally by "dilating" the all gray/white matter voxels through 12 cycles. Each cycle consists of expanding a volume of voxels to include all voxels lying directly adjacent to the prior volume. Thus, after several cycles, all sulci are filled in and the exterior surface becomes less convoluted, approaching that of the inner surface of the skull. The Laplace method can be applied to the volume between the new supracortical surface and the gray-CSF surface, resulting in a valuable one-to-one mapping. Because each cerebral hemisphere is nearly topologically equivalent to sphere, this method can effectively map the cortical surface onto a sphere (or any other sphere-like surface, such as the inside surface of the skull). Figure 6 shows a two-dimensional schematic of this method. The top panel shows a simple cortical hemisphere drawn as an oval with a large indentation representing a single deep sulcus. Sample points A through P are labeled on the cortical surface, and are equidistant from each other. The cortex is drawn with uniform thickness except near point D, and the thickness is coded by varying shades of gray. The supracortical volume is

externally bounded by a surface created by multiple iterations expanding the internal surface one voxel in each direction. As with the cortical analysis, the two surfaces are set to different boundary conditions and Laplace's equation is solved in between. After computing normalized gradients from Laplace's solution, streamlines are computed as shown by the lines connecting points A to A′, B to B′, etc. The streamlines can be interpreted as a one-to-one mapping of points from the cortical surface to the supracortical surface.

The advantage of the supracortical application is that each point on the cortical surface is associated with a pathlength representing the "depth" of that cortical element with respect to the supracortical surface. This provides some measure of cortical geometry, particularly about its folds and convexities. Furthermore, it becomes possible to correlate various cortical quantities with respect to cortical depth. For example, the variation of cortical thickness with cortical depth can be evaluated.

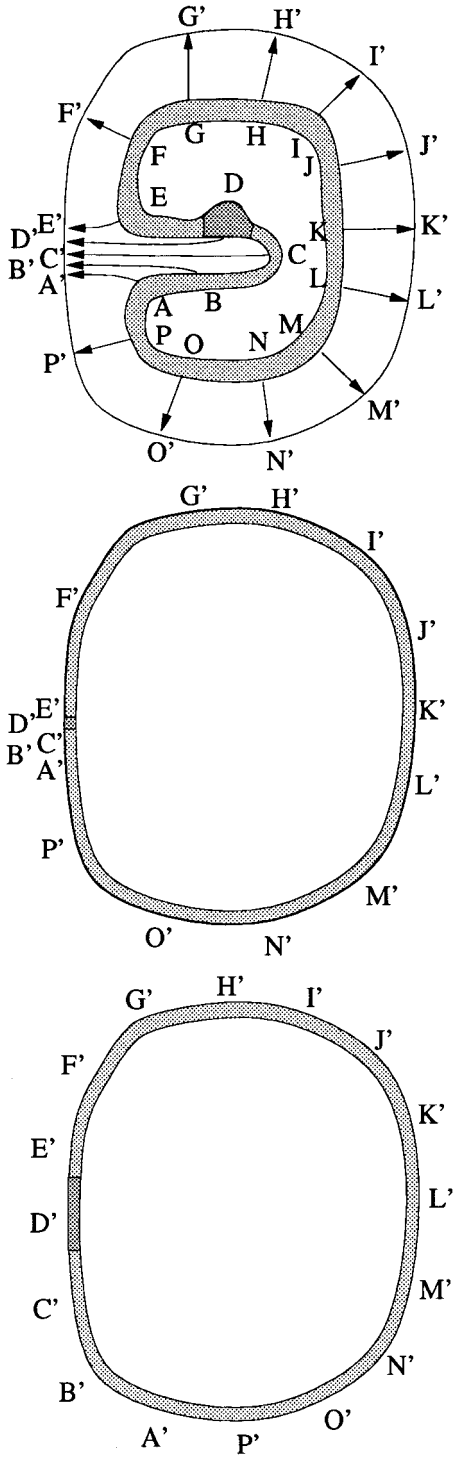


**Figure 6.**

Two-dimensional cartoon showing the application of Laplace's method to an extracortical volume. The top panel schematically shows one hemisphere with one large sulcus, labeled by points A through P spaced equidistant along the cortical surface. The thickness of the cortex is coded by shades of gray, for example, the dark shade at D reflects increased thickness. Laplace's method is applied to the extracortical volume defined between the cortical surface and a smoothed extracortical surface. Field lines from Laplace's method connect the two surfaces (e.g., lines A–A′, through P–P′). Note the points A′ through P′ are no longer equidistant. The middle panel uses the field lines to translate the coded cortical thickness from the cortical surface to the extracortical surface. Thus, the thicker cortex at point D is mapped as a correspondingly darker shade at point D′. The bottom panel results from warping the points from the middle panel so they are now equidistant. The darker shade mapped at point D′ is now easily visualized.

### Tomographic display method

The final result of the Laplace computation is a three-dimensional volume of numbers, one for each voxel in the cortical volume. Because the analysis is three-dimensional, the amount of data produced is considerable, and presentation of meaningful results becomes a significant task. One approach is a tomographic presentation of the cortex that is color-coded to represent cortical thickness.

A cartoon example of the tomographic approach is presented in the middle and lower panels of Figure 5. The middle panel displays an imaging plane intersecting the cortex and labeled the "observation plane." Consider the line connecting points A to A′ which, for example purposes, measures 2.8 mm in length. Because point A is below the observation plane and point A′ is above the plane, the line A–A′ must cross the plane as indicated at the point between the 7,500 V

and 2,500 V surfaces. Now consider the bottom portion of the Figure 5, which shows only the observation plane face-on. The lines of intersection of the observation plane with the gray-CSF surface and the gray-white surface are seen as the quasi-parallel curved lines. The area between those two lines represents the intersection of the cortical volume with the observation plane. That area is coded in shades of gray, with respect to the scale at left, representing the length of streamlines passing through any point. For example, the point corresponding to the intersection of the line A–A′ with the observation plane is indicated in the bottom panel by an arrow. Because the line A–A′ measures 2.8 mm in length, the shade of gray at that point corresponds to 2.8 mm in the gray scale.

### Surface-rendering display method

Another approach to present meaningful results is a rendering of the visible surface of the brain from an external projection. Again, the surface can be color-coded to represent cortical thickness, in case corresponding to the outermost voxels in the cortical volume. The drawback of this approach is that nearly 80% of cortex lies inside sulci, which is not visible to an outside observer. One solution is to include those internal voxels by mapping all voxels to a supracortical surface. Such a technique was described earlier, and a two-dimensional example is illustrated in the middle panel of Figure 6. Because the supracortical surface lacks the sulcal fold of the cortical surface, the points A′ through P′ are no longer equally spaced around the perimeter. The mapping warps the streamlines such that they are focused where the sulcus opens toward the supracortical surface. Notice that all of the cortical points between A and E are mapped into the short supracortical interval between A′ and E′. Furthermore, the streamline mapping translates the thickness-shading of the cortical surface to the supracortical surface. For example, the dark shade representing the thicker cortex at point D corresponds to the same dark shade at point D′. A surface rendering of the supracortical surface now visualizes information from all voxels associated with the external surface of the cortical volume. However, points on the supracortical surface are no longer equidistant, and details about the cortex originating within sulci are compressed and not easily visualized.

### Cortical-warping display method

Visualization of sulcal details on the supracortical surface can be recovered by warping points on that surface so they become equidistant. For example, in the bottom panel of Figure 6, visualization of details from A′ to E′ is increased by warping all points A′ through P′ so they now become equidistant. A surface rendering of the warped supracortical surface now reveals and resolves all voxels formerly hidden within the sulcal depths and compressed within a narrow region.

The warping algorithm is applied to three-dimensional MRI data by modeling each mapped voxel on the supracortical surface to have a positive electric charge such that it repels nearest neighbors. Nearest neighbors are defined on the original cortical surface as those directly adjacent to each other. Mathematically, the mean field of nearest neighbors is computed for each mapped voxel using an inverse potential. That is, the energy between any two nearest neighbors is inversely proportional to the distance between them. The mapped voxel moves proportionately in response to the mean field of all nearest neighbors, kinematically equivalent to motion dominated by high viscosity. The mapped voxels are constrained to move on the supracortical surface. All voxels are moved in parallel, and new fields are computed, and the process is repeated iteratively until the system reaches equilibrium. The approach to equilibrium is measured by the total system "energy" which is the sum of all nearest neighbor energies. This algorithm is not optimized and represents the most time-consuming portion of the analysis. This technique is related to an earlier one successfully developed by Dale et al. [1993] and refined by Fischl et al. [1999].

### Data acquisition

The success of any method measuring cortical thickness depends on the quality of the imaging data, which should meet the following three criteria. The first is to utilize all three dimensions evenly and fully because the brain is three-dimensional and has no preferred axis or orientation. The second criteria are to use sufficient resolution so that the thinnest cortex can be spanned by at least several voxel elements. For example, if the thinnest cortex is of the order 1 mm, then we require voxel sizes of 0.5 mm or smaller. The third criterion is sufficient contrast between the gray matter, white matter, and CSF so that the cortex can be reliably segmented. These goals are satisfied by the use of state-of-the-art MRI using high resolution,

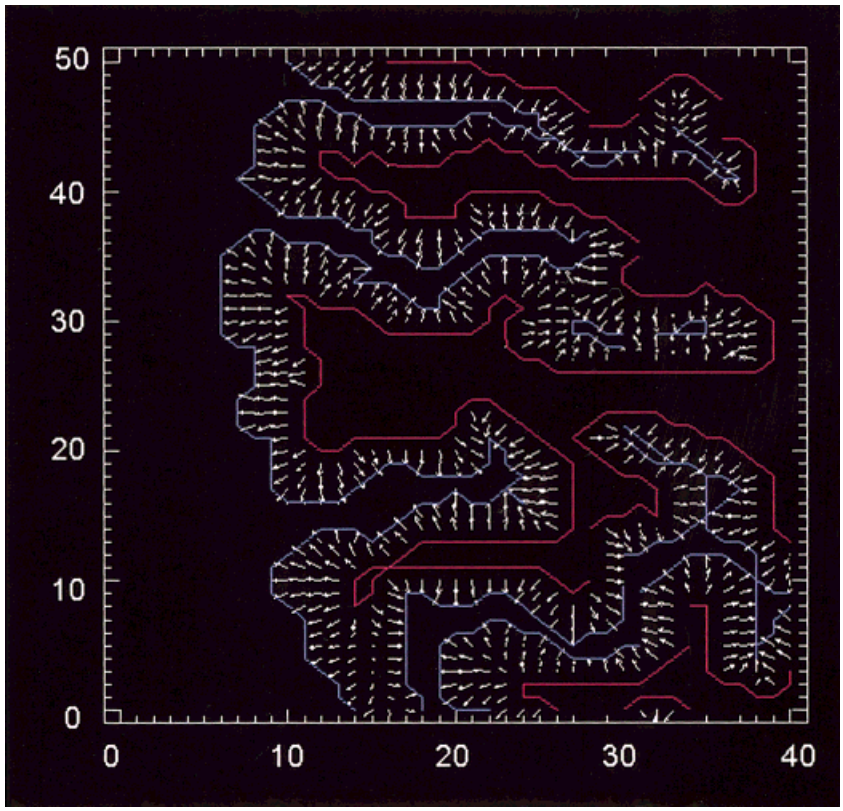


**Figure 7.**
Close-up example of gradients of Laplace's solution in an axial plane from real data. The blue line represents the gray-white junction, and the red line represents the gray-CSF junction. The small arrows are projections of the gradient vectors in the axial plane. These arrows are tangent to the streamlines connecting the two surfaces. Arrows appear short when they are projecting predominantly out of the axial plane [e.g., at position (15,5)]. The gradients are insensitive to small segmentation errors as seen but the sulcal discontinuity at position (30,29).

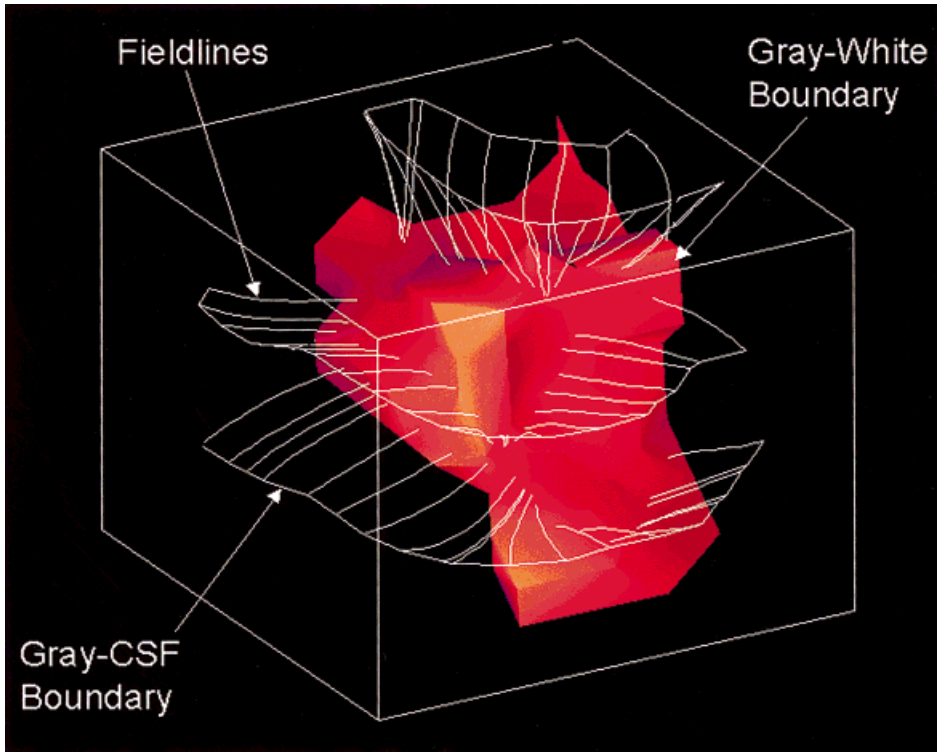


**Figure 8.**
Close-up of three-dimensional example of cortical volume from real data. The volume of data is roughly 10 × 10 × 10 voxels. The red surface is the gray-white surface from a sulcal bank on the lateral aspect of one hemisphere. The three continuous curvilinear lines are intersections of three axial planes with the gray-CSF surface, and thus lie on the gray-CSF surface. The connecting lines are examples of streamlines using the Laplace method. The cortical thickness at any point in the cortical volume is defined as the length of the streamline passing through it and connecting the two surfaces.

three-dimensional data acquisition algorithms on a T1 sequence.

Data were acquired using the 1.5 T and 3.0 T scanners at the NMR center of the Massachusetts General Hospital (Charleston, MA, USA). Although both normal and abnormal brains were scanned, this paper only presents the analysis from multiple scans on one brain as a proof-of-principal for the Laplace technique. Results from applications to abnormal neuroanatomy will be presented in a forthcoming paper.

The scans for this paper were performed on a General Electric Signa 1.5 T scanner. Sagittal T1 weighted images were acquired using a 3D SPGR sequence, employing IR preparation, variable bandwidth, and extended dynamic range, with TR 19 msec, TE 3.8 msec, TI 300 msec, flip angle 25, FOV 25 cm, slice thickness 1.2 mm, 124 slices, and 1 NEX. Although both low resolution (256 $\times$ 192) and high resolution (512 $\times$ 192) acquisition matrices were used, only the high-resolution results are presented here. The acquired voxel resolution was 0.5 mm $\times$ 1.3 mm $\times$ 1.2 mm. The data was interpolated to form cubic voxels with an edge length of 0.5 mm. Two 9-min and 43-sec scans were obtained and averaged together.

## RESULTS

An example of the field vectors from the Laplace solution from one small section of an axial slice is shown in Figure 7. At every grid point within the solution space of the cortical volume is a small arrow representing the component of the direction vector in the plane of the figure. As expected, the vectors all point in a smooth manner from the internal gray-white surface to the external gray-CSF surface. The thickness associated with any grid point can be calculated by following the direction of the vectors in both directions until the boundaries are reached. The thickness is defined as the total length of the path between the boundaries. Although Figure 7 is a two-dimensional slice for display purposes, the algorithm is computed three dimensionally as revealed by short arrows indicating vectors pointing out of the plane of the figure, such as at Cartesian coordinates (15,4).

Figure 7 also demonstrates the difficulties of segmenting the sulci and the insensitivity of the Laplace method to small errors. Notice that the end of the sulci at (32,29) is not directly connected to the beginning of the sulci. The segmentation routines have failed to completely resolve the sulci, leaving several sulcal islands. Such gaps cause errors of a factor of two in any definition of thickness based on the direct trajectory from one boundary to the other. An advantage of the Laplace method is that the overall solution is insensitive to the effect of gaps if they are small enough. Notice the direction vectors at (31,27) point as if a sulcal gap does not exist. Mathematically, the Laplace solution computes a saddlepoint that effectively bifurcates the cortical region as if a sulcus was continuous. A pathlength can still be calculated by taking advantage of the nonzero step size used to integrate the streamline. In the limit of zero step size, as the streamlines approach the saddlepoint they quickly turn away and never cross it. If the step size is sufficiently large, the integrated streamlines fail to make the turn and the saddle is crossed, effectively stepping across the gray-CSF surfaces and into the opposing face of cortex. This condition can be used to terminate the pathlength calculation, resulting in a reasonable approximation for the thickness as if the sulcal gap did not exist. Overall, we must balance the between the errors of integrating with a larger step size with that of an imperfect segmentation.

Figure 8 is an enlarged three-dimensional rendering of a small portion of cortex showing how the Laplace solution inherently solves for field lines in three dimensions. The red surface is the gray-white boundary. The three curved lines are the intersection of three axial planes with the gray-CSF junction. At intervals along these lines are many examples of field lines that connect the gray-white junction according to the Laplace solution. The inherent three-dimensional solution becomes manifest as the field lines twist in space according to the direction of the cortical volume. The length of any field line is used to define the cortical thickness in the region of that line.

After solving the Laplace equation, the cortical thickness is calculated and mapped at every grid point within the cortical volume by calculating the pathlength of the streamline that passes through that grid point connecting the gray-CFS surface to the gray-white surface. The thickness mapping is presented tomographically in the three cardinal planes as shown in Figure 9. The thickness in millimeters at any point within the cortex is color-coded with respect to the color bar on the right. Green-yellow colors represent cortex about 3 mm thick, whereas the dark blue colors represent cortex is about 1 mm thick.

A known neuroanatomical variation is the marked difference of thickness between the precentral gyrus and the postcentral gyrus [Meyer et al., 1996]. The axial image in Figure 9 shows the posterior bank of the central sulcus as visibly thinner than the anterior bank. To quantify the difference, each bank was sampled over 20 random locations. The anterior bank had a mean thickness of 2.8 mm (sample range of 2.5 to 3.5)

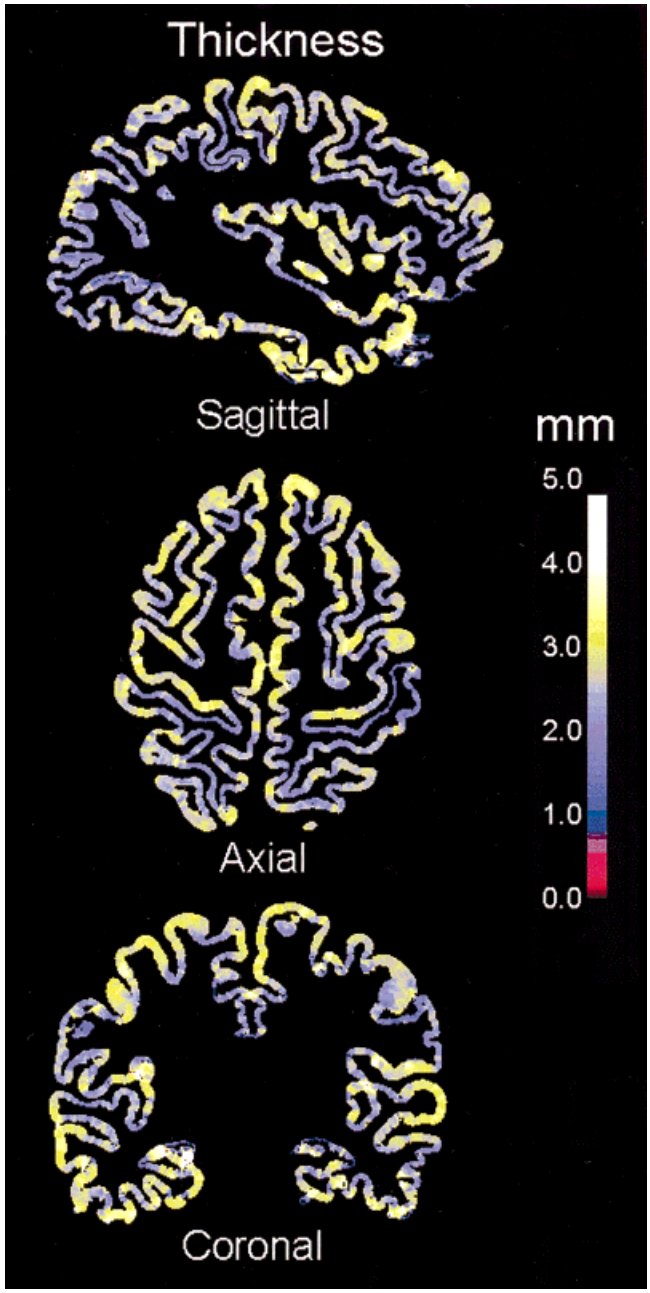


**Figure 9.**
Tomographic mapping of cortex to cortical thickness. The cortical volume is color-coded for thickness such that red, blue, green, and yellow regions are 1, 2, 3, and 4 mm thick, respectively. The images are from the three cardinal planes of the left hemisphere from one scan.

whereas the posterior bank had a mean thickness of 1.9 mm (sample range of 1.2–2.4). Although the left hemisphere was slightly thinner than the right hemisphere at the central sulci, the ratio of the anterior bank to the posterior bank was 1.50 for each hemisphere. This ratio is the same as presented by Meyer et al. [1996], using a MR technique focusing only on the central sulcus.

A statistical analysis of the cortical thickness is presented by the histogram in Figure 10. The vertical axis is a logarithmic scale of the relative frequency of cortical thickness with respect to the mode. The left and right hemispheres are analyzed separately as a self-consistency check. The cortex used for the Laplace solution has a computational volume of 3.75 million voxels, representing a real volume of 457 $cm^3$. The mean thickness is 2.69 mm for the left hemisphere and 2.67 mm for the right, which implies the total cortical surface area is 1702 $cm^2$. The median thickness for the left and right hemispheres is 2.52 mm and 2.49 mm, respectively. The median and mean differ by only 6%, implying the tail provides a small deviation to the mean. The standard deviation about the mean thickness is 0.61 mm. The thinnest 1% is less than 1.4 mm thick, and the thickest 1% is more than 4.5 mm thick. The origin of the thick "tail" is not clear, because it could result from segmentation errors at the bottom of gyral folds where the sulcus is not resolved.

Although a tomographic presentation is useful to examine the thickness of specific cortical regions, global variations along the surface are difficult to appreciate in a single slice. An alternative presentation is a simple surface rendering from an external viewpoint, as presented in Figure 11. The thickness of the external-most voxels is color-coded similarly to that of Figure 9. Topological landmarks are more easily seen, such as the central sulcus and Sylvian fissure. Global patterns in thickness are appreciated, such as a thinner postcentral gyrus, thicker precentral gyrus, and a thicker temporal lobe.

A correlation can be computed between the original cortical thickness and the sulcal depth. Figure 12 shows a color-coded contour plot constructed from juxtaposed histograms of cortical thickness at each sulcal depth. Each histogram is normalized to unity at each sulcal depth. The sulcal depth is calculated from applying the Laplace method to the supracortical volume. Because the supracortical surface lies a few millimeters off the superficial cortical surface, an additive constant is subtracted from all sulcal depths to renormalize all values so that superficial cortex is defined as zero depth. This provides the useful interpretation that any cortex with nonzero depth lies within a sulcus, and the higher the value the greater the depth. The lightest green color indicates the most common cortical thickness at that sulcal depth. The seven contours are spaced evenly between 0.9 and 0.3. At the

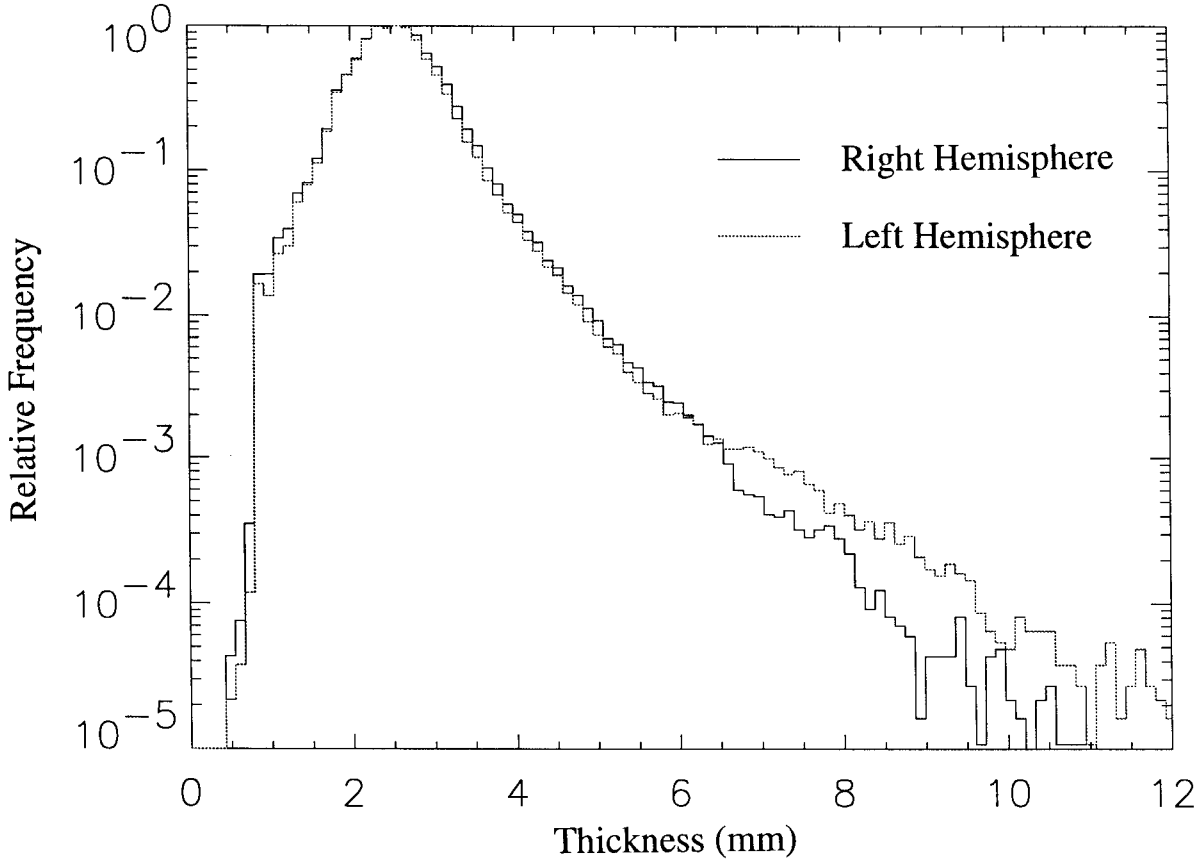


**Figure 10.**

Logarithmic histogram of frequency of cortical thickness from all calculated pathlengths, segregated by hemisphere. The most prevalent thickness in each hemisphere is about 2.5 mm. The falloff for both thinner and thicker cortex is nearly exponential. Significant differences between the hemispheres are not discernable. Thickness much larger than 7 mm are likely due to segmentation errors.

surface of the cortex (zero sulcal depth), the mean thickness is about 2.63 mm, whereas at any cortex deeper than 8 mm, the mean thickness decreases to 2.30 mm, a reduction of 14%. This result is concordant with known neuroanatomy [Meyer et al., 1996], and serves as further validation for the Laplace method.

Figure 13 shows a high resolution image equivalent to Figure 11 with the addition of the warping algorithm. Both lateral and medial surfaces are shown for each hemisphere. Details within the sulcal folds are now revealed on the surface, whereas they were completely buried in Figure 11. In effect, the cortical surface has been "inflated," a procedure pioneered by Dale et al. [1999] using a different method. The posterior bank of the central sulcus is clearly seen on both lateral surfaces as a dark band near the superior border, reflecting an absolute thinness with respect to the anterior bank. The visual cortex of the calcarine sulcus is also seen as a darker band on the posterior aspect of the medial surfaces.

Figure 14 presents cortical thickness and sulcal depth of the warped supracortical surface, together in one image. The sulcal depth is color-coded with respect to the color bar, so that red represents cortex originally lying on the superficial aspect of the brain, and green to yellow represents cortex originally lying deeper within sulci. Because the warping method has evenly spaced the mapped voxels over the supracortical surface, the ratio of cortex within and outside of sulci is readily apparent by the amount of red with compared to yellow-green. Lastly, any mapped voxel associated with thin cortex (defined as the lowest 20% of all thickness measurements) is displayed with an overlying white dot. Regions of thin cortex give the appearance of white clouds. The posterior bank of the central sulcus is easily seen as a continuous white band on the superior aspect of the lateral images. The

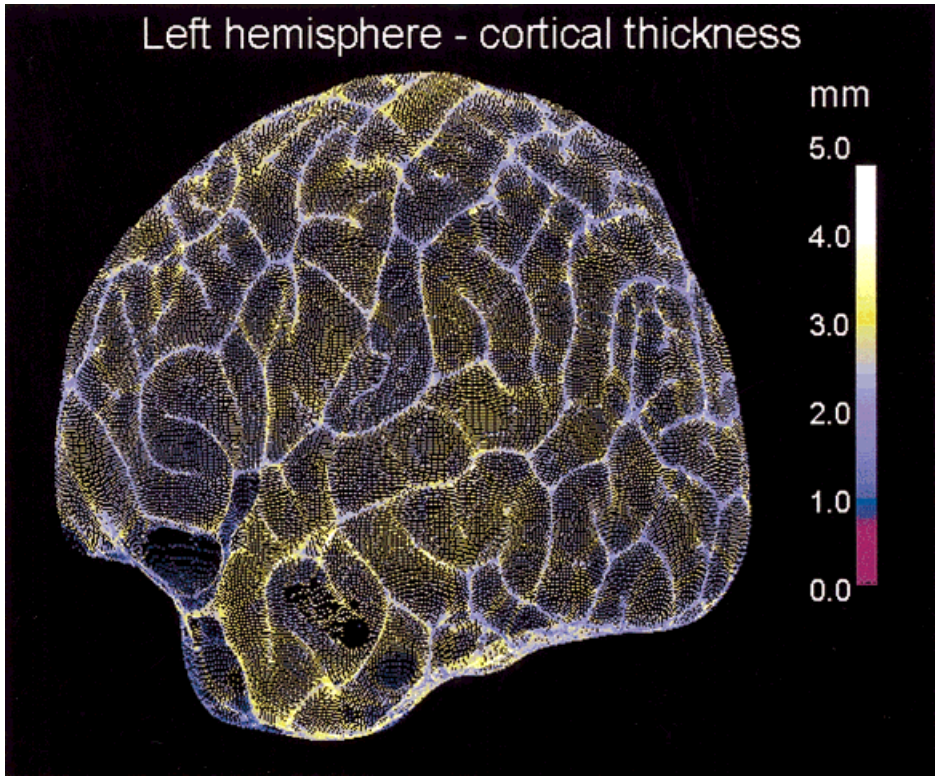


**Figure 11.**
Lateral view of superficial surface of left hemisphere with a color-coded mapping for cortical thickness. The color bar indicates any red, blue, green, and yellow cortex as being 1 mm, 2 mm, 3 mm, and 4 mm thick, respectively. The view is a direct projection of the externally visible and unwarped cortical surface, therefore, all mappings associated with sulcal cortex are not visualized. The high density of voxels lying on the sulcal banks visualizes the sulci. The defects at the anterior aspect of the temporal lobe are due to segmentation errors arising from the orbits.

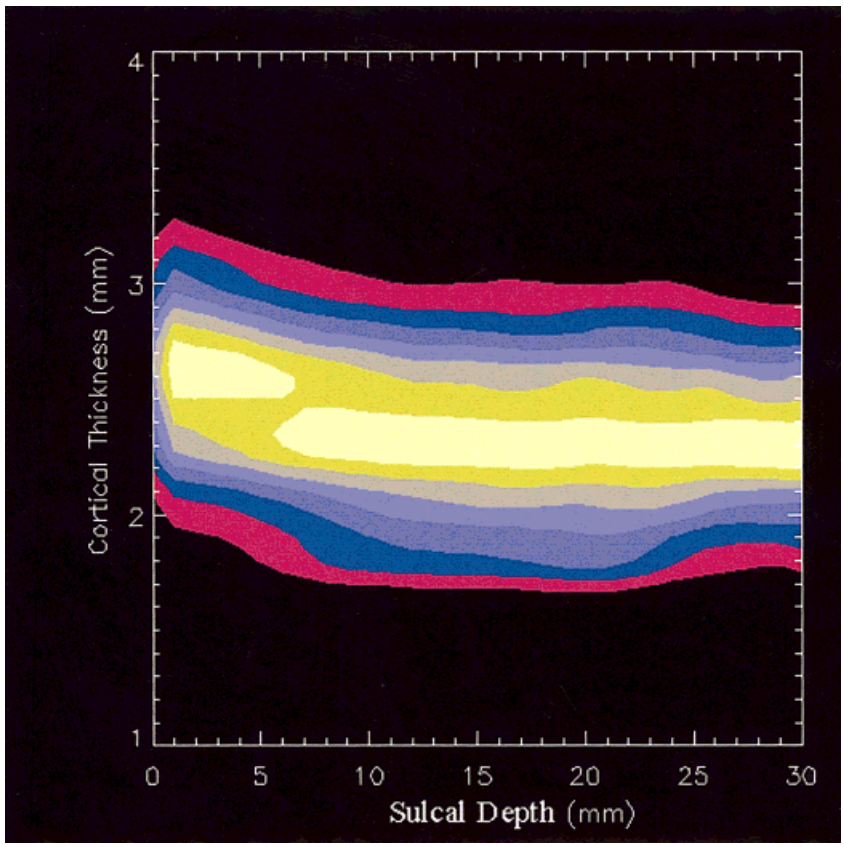


**Figure 12.**
A color-coded contour plot shows the relationship between cortical thickness and sulcal depth. At each sulcal depth, a histogram of all cortical thickness is obtained. Each histogram is normalized to unity. The histograms are then "stacked" together to form a mathematical matrix that can be visualized as a two-dimensional contour plot. There are seven contours at levels between 0.9 and 0.3. Bright colors (white-yellow) at the highest contours reveal the most common cortical thickness at each sulcal depth. The downward trend of all contours from 2.63 mm in the superficial cortex to 2.30 mm in the interior cortex is interpreted as a 14% reduction in cortical thickness with cortical depth. The transition is mostly complete for cortex deeper than 6 mm.

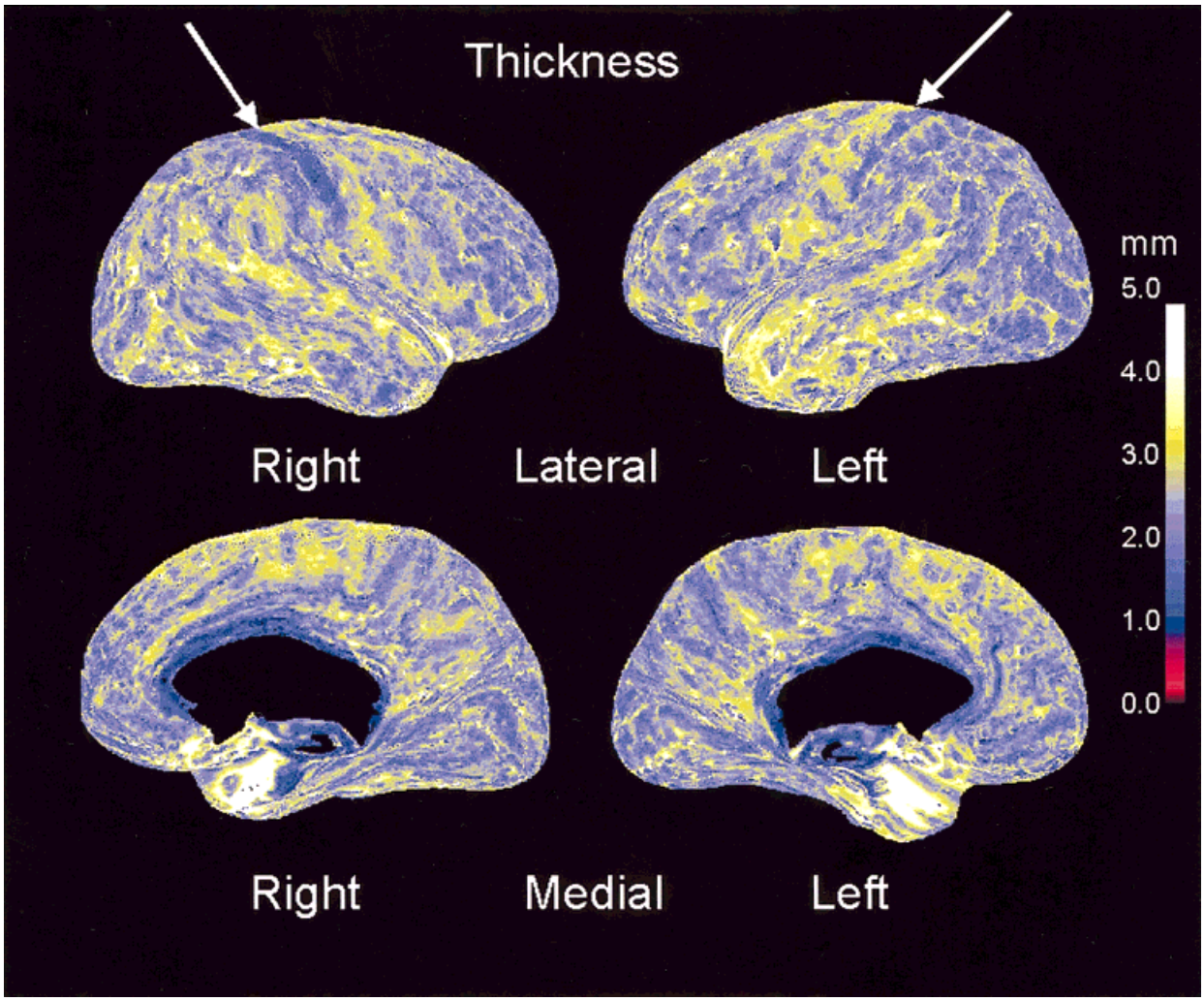


**Figure 13.**

Color-coded mapping of cortical surface with cortical thickness. The cortex has been warped to improve visualization by flattening the sulcal geometry to an smoothed extracortical form while approximately conserving relative cortical surface areas. The color bar codes for cortical thickness such that red is 1 mm thick and yellow is 4 mm thick. This highlights the relative thinness of the posterior bank of the central sulcal that is seen as a dark band emanating from the superior aspect of both lateral projections. The four views are from one scan which represent medial and lateral views of the left and right hemisphere.

general thickness of superficial cortex is revealed by the absence of white dots from cortex displayed as red. Both of these observations are corroborated by known neuroanatomy and serve to further validate the method.

## DISCUSSION AND CONCLUSIONS

This paper has presented a method based on Laplace's equation that can accurately compute a measure of the 3-D cortical thickness anywhere in the brain, given an accurate segmentation. Although cortical thickness measurements have been presented before [see Paxinos, 1990], they have suffered three drawbacks. First, they measure only a limited number of points throughout the cortex, sometimes only focusing on the central sulcus [Meyer et al., 1996]. Secondly, the standard measurements for reference are very old and were conducted on postmortum brains that were fixed, a process resulting in undetermined shrinkage. Lastly, these methods all employ a straight-line definition for thickness, which although valid in flat cortical regions, fails in highly curved or irregular regions. As such, the cortical thickness results pre-

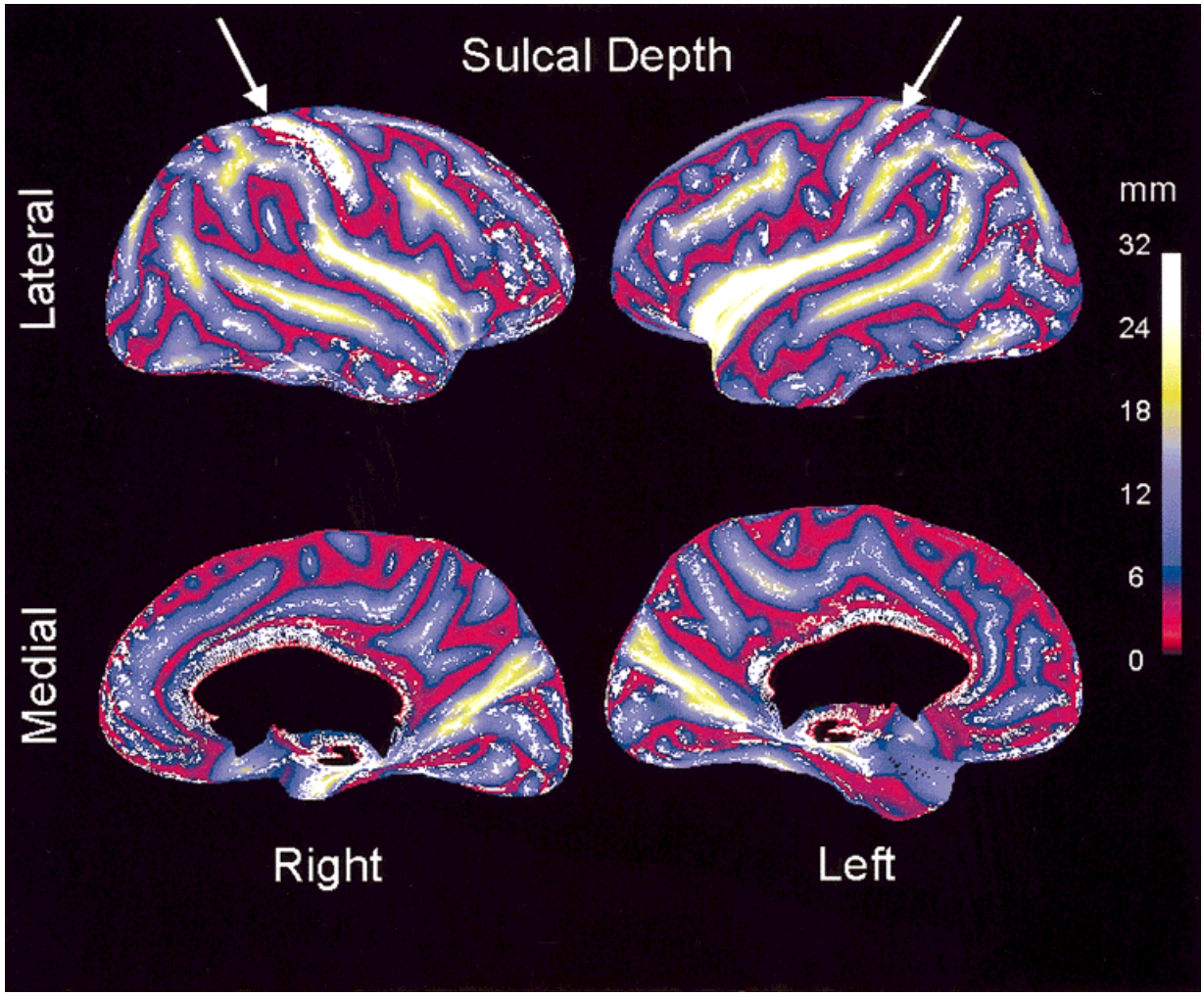


**Figure 14.**

Color-coded mapping of cortical surface with sulcal depth. The cortex has been warped to improve visualization by flattening the sulcal geometry to an smoothed extracortical form while approximately conserving relative cortical surface areas. The color bar codes for sulcal depth relative to the superficial cortical surface such that any non-red color represents cortex lying within sulci. White dots are superimposed over any region of cortex that is thinner than 1.2 sigma of the mean thickness. This highlights the association between sulcal cortex with thinner cortex. The four views are from one scan which represent medial and lateral views of the left and right hemisphere.

sented in Figure 14 are the first in vivo measurements incorporating the entire brain.

The only approach at present to validate the Laplace method is to corroborate cortical thickness results with that of established variations in neuroanatomy. Here we focus on two well-known variations, the first involving the banks of the central sulcus, and the second involving decreasing thickness with sulcal depth. The first variation is supported by Figures 10 and 14, which show the relative thickness of the anterior bank over the posterior bank to be in the ratio of 1.5, in agreement with Meyer et al. [1996], and the references therein. The second variation is supported by Figure 12, which shows the percentage decrease in cortical thickness from the cerebral surface (2.63 mm) to the interior (2.30 mm) to be 14%.

The Laplace method was successfully tested initially on a contrived dataset representing the brain as a sphere, with a cortex lying as an outer shell. Because the cortical thickness was determined exactly a priori, the computational noise and accuracy of the method could be evaluated independently from that due to

real MRI data from a real brain. Next, the method was tested by comparing results from two scans of the same brain at different resolutions, 256 × 256 vs. 512 × 512. Both methods showed the same variations, particularly about the central sulcus and with sulcal depth. The lower resolution scan yielded slightly more noisy results, although the mean thickness was about the same. The 512 × 512 data is felt to be more accurate for the following reason. The mean cortical thickness is about 2.5 mm, and the voxel sizes for the 256 × 256 and 512 × 512 scans are 1.0 and 0.5 mm, respectively. Thus, the cortical thickness is spanned on average by 2.5 voxels with low resolution, and with 5 voxels with high resolution. The difference from 2.5 to 5 voxels is felt to be a significant increase in local computational accuracy, although the global accuracy is comparable.

Although the figures presented in this paper are from one analysis of a normal brain, three other brains were scanned and analyzed. One brain was scanned at low resolution (256 × 256) with detailed corrections removing MRI signal gradients. The last two brains were abnormal with known cortical thickness pathologies causing focal epilepsy. These results will be presented in a forthcoming paper detailing the application of the Laplace method to abnormal brains. All three scans showed cortical variations consistent with that presented in this paper, namely the relative thin and thick cortex on the respective posterior and anterior banks of the central sulcus, and the relative thinning of the cortex with increasing sulcal depth.

Errors in the pathlength along a specific streamline have three origins. The first is integration of the gradient of the Laplace potential which determines the streamline. The streamline is determined by starting at some voxel within the cortex and walking along the gradient field in both directions until either the gray-CSF or gray-white boundaries are crossed. The accuracy of the pathlength can be no better than the step-length used in the integration, which was 0.25 of a voxel, or 0.125 mm, for the analysis presented earlier. The second source of error is the exact location of the gray-CSF and gray-white boundaries within the gridded array of voxels. Because the boundaries can never be a distance of more than $2a\sqrt{3}$ from a grid point (for a uniform grid where $a$ is the linear size of a voxel), a maximum possible error of 0.444 mm is possible. The errors described apply to the calculation of a single streamline and pathlength. The magnitude of the individual errors is reduced statistically by averaging the pathlengths from a large number of voxels within a cortical region. Because the entire cortex contains over 3.5 million voxels, each associated with one pathlength, the displayed pathlengths within the figures from any small region represent the averaging and overlap of a considerable number of single pathlengths. Also, a detailed comparison of neighboring pathlengths shows that the voxel-to-voxel variation tends to be quite small and ranges around 10%.

The third source of error is the segmentation that defines whether a voxel lies in the white matter, gray matter, or CSF, thereby defining the gray-CSF and gray-white surfaces. This is not an error in the Laplace method itself, only with the segmentation upon which it is analyzing. In fact, solving Laplace's equation is computationally robust once the cortical volume is established. Cortical segmentation is a thriving field of research and although we developed all of our own methods, they are not state-of-the-art and could be improved [Dale et al., 1999]. There are two types of segmentation errors, global and local. The global error occurs for inappropriate choices of segmentation thresholds. For example, if the choice of threshold for the gray-CSF surface is too low, then the cortex will appear globally too thick. Furthermore, the entire gray-CSF surface of a sulci may not be resolved leading to cortex that appears strangely nodular. On the other hand, if the choice of threshold for the gray-CSF surface is too high, then the cortex will appear globally too thin. Similarly if the gray-white threshold is too low, the cortical thickness will appear globally too thin, and if the gray-white threshold is too high, the cortical thickness will appear globally too thick.

Unfortunately there is no rigorous method to specify the exact thresholds for gray matter, and determination is based on the judgment of a trained eye examining overlaid contours on a raw MRI image. One alternative is analysis of the histogram of raw MRI data, particularly focusing on the positions, widths, and magnitudes of the gray matter and white matter peaks [Worth et al., 1997]. Threshold values can be specified at fixed positions with respect to those peaks, however, a trained eye is required to make those initial specifications. We feel the uncertainty due to systematic errors in segmentation is of order one voxel, or 0.5 mm in the present analysis. Another approach to assess the sensitivity to global segmentation errors is to conduct multiple analyses using different thresholds on the same data. For small changes (of order 10%) in the thresholds about an optimum, the overall pattern of cortical thickness was invariant, although the magnitude was rescaled (of order 5%).

Nonsystematic, or local, segmentation errors result from local variations in voxel intensity, which can be due to either noise in the MRI image, field gradient effects, volume averaging effects, or unresolved sulci where the opposing cortical banks are pressed together. In contrast to global segmentation errors, the Laplace method can be robust to local errors, particularly in deep sulci where the entire gray-CSF surface between opposing faces of cortex can be difficult to segment. Robustness is obtained by altering the endpoint criterion for the pathlength integration as described in the methods section. Although, strictly, the streamline should be integrated from the 0 V to 10,000 V surfaces, different values could be chosen for the endpoints. For example, in this paper, the integration endpoints are set at 500 V and 9,500 V. The advantage is that the 500 V and 9,500 V surfaces are less sensitive to local segmentation errors than the 0 V and 10,000 V surfaces. That is, these intermediate surfaces tend to smooth over segmentation mistakes and bridge segmentation gaps in the outermost boundary surfaces. This advantage is particularly evident in the gray-CSF surface deep within sulci where portions of the 10,000 V surface often fail to appear, as exemplified in Figure 7 by the discontinuous sulci at position (32,29). At such locations, there is no 10,000 V surface separating the opposing faces of the gray-white boundary, and one could mistakenly integrate a continuous streamline all the way across both sections of cortex. However, intermediate surfaces such as 9,500 V can fill in such gaps, thereby preventing this error. Although the cortical thickness will be rescaled globally to a slightly smaller value, the overall pattern of thickness variations should not be affected.

A possible method to overcome segmentation errors would be incorporation of an adaptive segmentation algorithm. Presently, applying intensity thresholds to each image segments gray matter. The same thresholds are used globally throughout the entire image. Segmentation errors due to signal variations could be reduced by an adaptive routine that corrects the gray matter boundaries by local examination of gray matter topology. This process is accomplished by the human eye which can easily discern the gray-white junction from a MRI scan which has superimposed local variations of signal strength. A simple computerized segmentation based on global thresholds fails in this case. An adaptive algorithm could mimic the human eye's computational ability by correcting a simplistic segmentation with local information from signal gradients.

A disadvantage of the Laplace method is that the entire analysis is computationally intensive, requiring about 24 h of computing time on a Sun Ultra II. However, the majority is spent during the algorithm that warps voxels on the supracortical surface whereas the Laplace solution requires only several hours. All algorithms are presently unoptimized and there is a large potential for increased speed. Computation of the cortical Laplace solution itself is relatively quick, requiring about 2 h for convergence, whereas the pathlength solution requires about 6 h. In the interest of timely development, we used the simpler Jacobi method, although significant improvement could be made using a Gauss-Seidel or Simultaneous Overrelaxation (SOR) method. Computation for the supracortical Laplace solution requires about 8 h due to stricter convergence criteria. It is essential to carefully track the long field lines extending from sulcal depth to the supracortical surface, which can be as long as 30 mm, as compared to the cortical thickness of about 3 mm. Considerable time is also spent de-shelling the cortex, which includes removing the skull, nerves, spinal cord, etc. This process is not automated because particular attention must is required to carefully remove tissues adjacent to the cortex to obtain a clean gray-CSF boundary. As such, this process requires significant human operator time. Although the total analysis time approaches several days, the entire process could be reduced to a few hours with experience and optimized routines.

Future work will focus on further validation of the method and building a database of cortical thickness from a population of normal and abnormal brains. One direct method of validation is to analyze a cadaveric brain by a point-to-point comparison of a postmortum MRI Laplace analysis with direct measurement of cortical thickness. Direct measurements would be taken at multiple locations where the cortical curvature is very low, thereby adopting a straightline distance as the measure of thickness. Motivation for this procedure is to rule out nonuniformities of the MRI signal which cause cranially interior signals to become hyperintense or hypointense. This effect could cause systematic variations in cortical thickness with sulcal depth which confound the known neuroanatomical variation. A second motivation for a cadaveric comparison is to develop relations between MRI thresholds for the gray-white and gray-CSF junctions (with respect to intensity histograms) and the anatomical junctions. This procedure can reduce systematic segmentation errors that were described earlier.

There are many advantages to building a library of cortical thickness maps from different brains with normal and abnormal anatomy. The first is to establish

what is the normal range of cortical thickness and what is the normal pattern of thickness variations along the cortex. Once this is established, normal correlations between thickness maps and parcelation maps [Caviness et al., 1996] can be studied for scientific interest in many aspects of neuroscience. Then for clinical interest, analysis correlating abnormal thickness with known pathology can be undertaken. Although there could be a danger of developing a neophrenology, legitimate clinical decision making could be based on patterns of abnormal thickness. An example is surgical excision of brain matter in patients with intractable epilepsy. Focal seizures are often known to be related to thickened cortex, and providing cortical thickness maps to a neurosurgeon would allow more careful planning and management. A second example could be enhanced diagnosis of Alzheimer's disease based on patterns of atrophy established by scanning a population of patients. There are also neuropsychiatric diseases which could have subtle signatures revealed as unique patterns of cortical thickness or thinness.

One advantage of the Laplace method is its generality. Although the Laplace method is applied here to the problem of cortical thickness, it could be applied to any imaging problem involving the thickness between two discernable and nonintersecting surfaces. The necessary data representation is a volumetric labeling of the three volumes: between the two surfaces, and on either side. Surfaces represented parametrically can easily be converted into this form. It is also essential that the volume between the surfaces be at least one voxel thick, with more voxels providing more accuracy. Possible applications could include evaluating (1) the cardiac wall in cardiomyopathy or infarction, (2) the intestinal wall as early indications of neoplasia or ulceration, or (3) cortical bone thickness in osteoporosis [Newman et al., 1998]. The limitations to these applications are signal contrast, image resolution, and computing power. The latter limitation will diminish with the inexorable progress of the computer industry, and imaging applications that now seem overly complicated will become commonplace and important tools in medicine.

## ACKNOWLEDGMENTS

We would like to thank Mark Bautz of the Center for Space Research at the Massachusetts Institute of Technology for allowing one of us (S.E.J.) to use their computer facilities and offices. We also thank Geoffrey Jones for a mathematical review, Colin Allen for the figures, and Anders Dale, Bruce Fischl, Dave Kennedy, Nikos Markis, and Andy Worth, of the Center for Morphometric Analysis at the Massachusetts General Hospital for many informative conversations and comments.

## REFERENCES

Apostol T. (1967): Calculus. New York, John Wiley & Sons.

Braitenberg V, Schuz A (1988): Cortical statistics and geometry of neuronal connectivity. Berlin, Germany: Springer-Verlag.

Bland D. (1965): Solutions of Laplace's equation. London, UK: Routledge & Kegan Paul.

Caviness V, Jr., Makris N, Meyer J, Kennedy D (1996): MRI-based parcellation of human neocortex: an anatomically specified method with estimate of reliability. J Cog Neurosci 8:566–588.

Dale A, Fischl B, Sereno M (1999): Cortical surface-based analysis I: segmentation and surface reconstruction. Neuroimage 9:179–194.

Dale A, Serene M. (1993): Improved localization of cortical activity by combining EEG and MEG with MRI cortical surface reconstruction: a linear approach. J Cogn Neurosci 5:162–176.

Double K, Happiday G, Kril J, Harasty J, Cullen K, Brooks WS, Creasey H, Broe GA (1996): Topography of brain atrophy during normal aging and Alzheimer's disease. Neurobiol Aging 17:513–521.

Fischl B, Sereno M, Dale A (1999): Cortical surface-based analysis II: inflation, flattening, and surface-based coordinate system. Neuroimage 9:195–207.

Grignon Y, Duyckaerts C, Bennecib M, Hauw J (1998): Cytoarchitectonic alterations in the supramarginal gyrus of late onset Alzheimer's disease. Acta Neuropathol (Berlin) 4:395–406.

Henery C, Mayhew T (1989): The cerebrum and cerebellum of the fixed human brain: efficient and unbiased estimates if volumes and cortical surface areas. J Anat 167:167–180.

Johnson L, Riess R (1982): Numerical analysis. Reading, MA: Addison-Wesley Publishing Co.

Kwon J, McMarley R, Hirayasu Y, Anderson J, Fischer I, Kilkinis R, Jolesz F, Shenton M (1999): Left planum temporale volume reduction in schizophrenia. Arch Gen Psychiat 56:142–148.

Lambe E, Katzman D, Mikulis D, Kennedy S, Zipursky R (1997): Cerebral gray matter volume deficits after weight recovery from anorexia nervosa. Arch Gen Psychiat 54:537–542.

Lef J, Andermann F, Dubeau F, Bernasconi A, MacDonald D, Evans A, Reutens D (1998): Morphometric analysis of the temporal lobe in temporal lobe epilepsy. Epilepsia 7:727–736.

Meyer J, Roychowdhury S, Russell E, Callahan C, Gitelman D, Mesulam M (1996): Location of the central sulcus via cortical thickness of the precentral and postcentral gyri on MR. AJNR Am J Neuroradiol 9:1699–1706.

Momenan R, Hommer D, Rawlings R, Ruttimann U, Kerich M, Rio D (1997): Intensity-adaptive segmentation of single echo T1-weighted magnetic resonance images. Hum Brain Mapp 5:194–205.

Morse PM, Feshbach H (1953): Methods of theoretical physics. New York: McGraw-Hill Book Company.

Newman D, Dougherty G, al Obaid A, al Hajrasy H (1998): Limitations of clinical CT in assessing cortical thickness and density. Phys Med Biol 43:619–626.

Paxinos G, editor (1990): The human nervous system. San Diego, CA: Academic Press.

Press WH, Teukolsky SA, Vetterling WT, Flannery BP (1992): Numerical recipes in C: the art of scientific computing. Cambridge, UK: Cambridge University Press.

Research Systems, Inc., IDL Reference Guide, Version 5.0, 777 29th Street, Suite 302, Boulder, CO 80303, (303) 786-9900.

Tanabe JL, Amend D, Schuff N, DiSclafani V, Ezekiel F, Norman D, Fein G, Weiner MW (1997): Tissue segmentation of the brain in Alzheimer disease. Am J Neuroradiol 18:115–123.

Toga AW, Goldkorn A, Ambach K, Chao K, Quinn BC, Yao P (1997): Postmortem cryosectioning as an anatomic reference for human brain mapping. Comp Med Imag Graph 21:131–141.

Von Economo C, Koskinas G (1925): Die cytoarchitektonik der hirnrinde des erwachsenen Menschen. Berlin: Springer.

Worth AJ, Makris N, Caviness VC, Jr., Kennedy DN (1997): Neuroanatomical segmentation in MRI: Technological objectives. Int J Pattern Recog Art Intell 11:1161–1187.

Zeng X, Staib LH, Schultz RT, Duncan JS (1999): Segmentation and measurement of the cortex from 3-D MR images using coupled-surfaces propagation. IEEE Trans Med Imag 10:927–937.